Vacuum Resonance States as Atomic-Scale Probes of Noncollinear Surface Magnetism

Anika Schlenhoff,* Štěpán Kovařík,† Stefan Krause, and Roland Wiesendanger
Department of Physics, University of Hamburg, Jungiusstrasse 11A, 20355 Hamburg, Germany

(Received 22 January 2019; published 23 August 2019)

The reflection of electrons at noncollinear magnetic surfaces is investigated by spin-polarized scanning tunneling microscopy and spectroscopy on unoccupied resonance states located *in vacuo*. Even for energies up to 20 eV above the Fermi level, the resonance states are found to be spin split, exhibiting the same local spin quantization axis as the underlying spin texture. Mapping the spin-dependent electron phase shift upon reflection at the surface on the atomic scale demonstrates the relevance of all magnetic ground state interactions for the scattering of spin-polarized low-energy electrons.

DOI: 10.1103/PhysRevLett.123.087202

Spintronic devices raise expectations for meeting future technological demands for ever smaller and more efficient devices, exploiting the electron spin rather than its charge. Here, understanding the spin-dependent scattering of electrons at magnetic interfaces and surfaces is of high relevance for the control of electron transport. It is therefore in the focus of numerous electron reflection studies [1–6]. However, atomic-scale variations of the scattering process, for example, on noncollinear magnetic surfaces, remained inaccessible, due to the laterally averaging nature of the established experimental approaches. In our spin-polarized scanning tunneling microscopy (SP-STM) experiments, we realize a spin-resolved electron vacuum interferometer on the atomic scale by placing a biased magnetic probe tip in front of a magnetic surface. Unoccupied electronic resonance states (RSs) evolve between the tip and the surface that are expected to be highly sensitive to the electronic band structure of the sample [7,8]. By tuning the bias, spin-polarized electrons from the tip are injected into individual RSs, and the resulting spin-resolved tunnel current is recorded. We find that all RSs are sensitive to the local spin quantization axis of the sample, indicating that the spin-dependent electron scattering at the surface is affected by the combined Heisenberg exchange, Dzyaloshinskii-Moriya (DM), and spin-orbit interactions.

The basic physical idea of the experiments is depicted in Fig. 1. As shown in Fig. 1(a), an electron interacts with a surface when being reflected. For the electron's wave function, a phase shift ϕ_C is introduced at the reflection point that is given by the surface electronic band structure [9]. When the electron is trapped by multiple reflections between the surface and the vacuum barrier, an additional phase shift ϕ_B is introduced, as depicted in Fig. 1(b). Within the context of a phase accumulation model, electron standing waves fulfilling the quantization condition

$$\phi_B + \phi_C = 2\pi n, \quad \text{with integer } n, \tag{1}$$

evolve as RSs [9–11]. In the absence of an electric field, the RSs in the Coulombic image potential are given by a Rydberg-like series of image-potential states (IPSs) [10,11]. With increasing electric field, the IPS experience a Stark-shift to higher energies [12–14]. In the limit of a very high electric field, the RSs evolve in an almost triangular electrostatic potential in front of the surface.

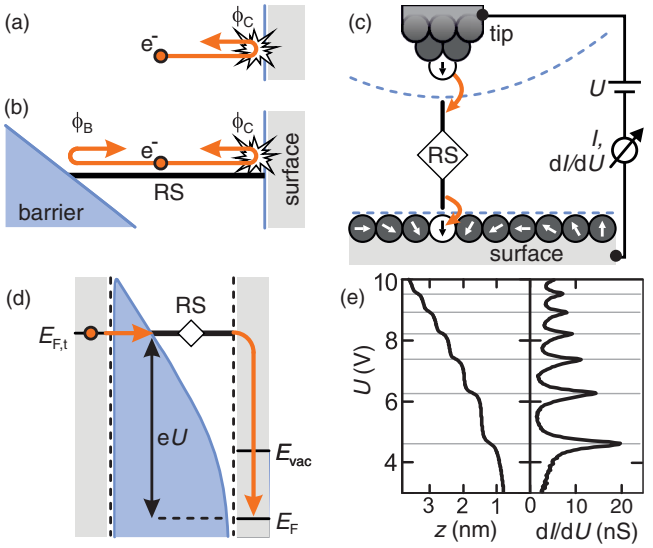

FIG. 1. Experimental approach. (a) Electron reflection at surfaces leads to a phase shift ϕ_C. (b) A resonance state (RS) is an electron wave trapped by multiple reflection between the vacuum barrier and the crystal surface, associated with phase changes ϕ_B and ϕ_C, respectively. (c) The net spin-polarized current I flowing from the tip via the RS to the sample and the differential conductance dI/dU is measured as a function of tip position and relative orientation of tip and surface spins. (d) Physical picture of electrons tunneling resonantly from the tip into a RS. (E_{vac}: surface vacuum level; $E_{F,t}$, E_F: Fermi level of tip and surface.) (e) Tip-sample displacement $z(U)$ and $dI/dU(U)$, revealing the first six RSs on the DL Fe/W(110) ($I = 2$ nA, $T = 40$ K).

In the following we will refer to them as field states (FSs).

Magnetic properties of the RSs are attributed to both the vacuum potential and the surface electronic band structure. The coupling to the spin-polarized band structure generates a significant energy splitting of the RSs, whereas the influence of the spin polarization of the vacuum potential was found to be negligible [15]. Consequently, any spin polarization of the RSs predominantly arises from the spin-dependent electron reflection at the magnetic surface.

Our experimental approach is depicted in Fig. 1(c). A magnetic probe tip at bias U is placed above a sample surface exhibiting a noncollinear magnetic texture, and spin-polarized electrons are injected into an individual RS. The resulting spin-resolved tunnel current I and differential conductance dI/dU signals are measured as a function of tip position. In Fig. 1(d), a physical picture of the experiment is shown. When eU corresponds to the energy of a RS, spin-polarized electrons tunnel from the magnetic tip into the unoccupied RS and subsequently relax to the surface. Because of the low electron lifetime in the RS, the time between consecutive electrons filling the RS is much larger than the time for the decay into the surface [13,16]. As a consequence, I and dI/dU reflect the tunnel current and differential conductance between the probe tip and the RS, and local variations therein correspond to local variations of the RS properties.

The experiments were performed under ultrahigh vacuum conditions with a pressure below 1×10^{-8} Pa using a home-built SP-STM at variable temperatures. Within the experimental setup, the entire microscope including the tip was cooled to maximize the thermal stability. Antiferromagnetic bulk Cr tips were used to avoid an undesired dipolar coupling with the sample [17]. Simultaneously to the constant current topography images at closed feedback loop, a small ac modulation voltage ($U_{\mathrm{mod}} = 40$ mV, $f = 4.333$ kHz) was added to the applied bias voltage U in order to record the spatially resolved differential conductance dI/dU by lock-in technique.

In order to identify the RSs, scanning tunneling spectroscopy was performed on the sample surface [12,18]. A spectrum recorded on the double layer (DL) Fe on W(110) is shown in Fig. 1(e). Here, a feedback control unit regulates on a constant current between the probe tip and the sample by adjusting the tip height z while ramping U. Note that I is predominantly governed by Fowler-Nordheim field emission for eU being larger than the sample work function [8]. Consequently, the feedback loop regulates on an approximately constant electric field at the tip, resulting in a tip retraction when increasing U. For U corresponding to an RS energy, an additional transmission channel opens, resulting in a local peak in dI/dU and a step in $z(U)$, as observed in Fig. 1(e).

In Fig. 2(a), an SP-STM image is shown, taken on the DL Fe/W(110) and using spin-polarized tunneling into the

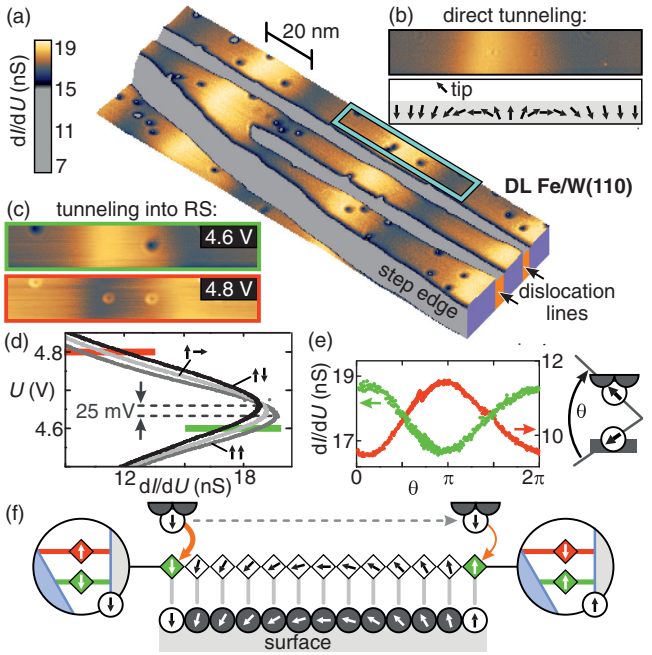

FIG. 2. Magnetic imaging via spin-polarized tunneling into the first RS. (a) Three-dimensional view of the DL Fe/W(110) sample surface colored with the magnetic dI/dU map ($U = 4.6$ V). (b) dI/dU map of the area marked in (a), recorded by direct tunneling into the surface ($U = 0.3$ V). Arrows indicate the local spin texture (side view) and the tip magnetization direction. (c) dI/dU maps recorded on the same area as in (b) at indicated bias, revealing an inversion of the magnetic contrast. (d) dI/dU spectra, taken on spots with different relative spin configurations between the tip and the sample, as indicated. Bias voltages of (c) are marked. (e) Magnetic signal $dI/dU(\theta)$, as extracted from (c). (f) Physical picture: the RS spin quantization axis rotates locally with the underlying spin texture, while the energy positions of majority and minority RS are preserved. ($I = 2$ nA, $T = 40$ K.)

first RS. In the z channel, two dislocation lines are visible that relieve the strain in the atomically flat Fe film. Additionally, a mono-atomic step edge is visible, caused by a step on the W(110) substrate. The topography is colored with the simultaneously recorded map of the dI/dU signal. From SP-STM studies using spin-polarized tunneling directly into the sample, the DL Fe/W(110) is known to exhibit a periodic magnetic domain pattern with Néel-type domain walls of unique rotational sense [19,20]. While the magnetization of the ferromagnetic domains points perpendicular to the film plane, the magnetic moments in the domain walls rotate through the film plane. In Fig. 2(b), a magnetic SP-STM image of the area marked in Fig. 2(a) is shown, recorded with spin-polarized tunneling directly into the surface. For spin-polarized tunneling, the dI/dU signal varies with the cosine of the enclosed angle between the magnetization directions of the tip and the sample [21,22]. Fitting an established model of 180° domain walls to the data allows the determination of the

spatial evolution of the surface spin texture [19,23,24], as indicated in Fig. 2(b). A dI/dU map, generated by spin-polarized tunneling into the first RS on the same area, is shown in Fig. 2(c). It reveals the same magnetic pattern as in Fig. 2(b), indicating that the lateral evolution of the RS reflects the spin texture of the surface. Consequently, the RS can be used for spin-resolved imaging, as shown in Fig. 2(a). When slightly changing the bias, the magnetic contrast inverts, as shown in Fig. 2(c). Local spectroscopy curves taken on different spots on the surface for parallel, orthogonal, and antiparallel alignment of tip and sample magnetization reveal that the $dI/dU(U)$ curves shift slightly, as shown in Fig. 2(d) [24]. Such a shifting has been observed before and is a consequence of the large energy overlap between majority and minority RSs due to their small exchange splitting relative to their intrinsic line widths [13,16,25,26]. For finite spin polarization, tunneling occurs simultaneously into both the majority and the minority RS, effectively resulting in a single spectroscopic peak that shifts to lower (higher) energies for the parallel (antiparallel) alignment of tip and sample magnetization [24]. As a consequence, when changing the bias from the rising to the falling flank of the spectroscopic peak, the magnetic contrast inverts, as demonstrated in Fig. 2(c). Based on the shifting of the peak position, an effective splitting can be determined, resulting in approximately 25 meV. Assuming a spin polarization of the tip of roughly 40%, this value is in accordance with previous experiments [16,26–28].

In Fig. 2(e), the dI/dU signal is plotted as a function of relative spin phase θ between tip and sample, based on the spatial evolution of the spin texture shown in Fig. 2(b). Obviously, the dI/dU signal scales with $\cos(\theta)$, being a manifestation of the imaging function for spin-polarized tunneling [21,29]. The implications of this finding for the spin-dependent properties of RSs are depicted in Fig. 2(f). The RS exhibits a spin quantization axis that is parallel to the local surface spin. On surfaces with the spin quantization axis changing with lateral position, the spin quantization axis of the RS rotates with the underlying spin texture, while the energy positions of the majority and the minority RS are preserved. Depending on the applied bias, spin-polarized tunneling occurs predominantly into the majority or the minority RS.

The question arises whether the local spin quantization axes of the RSs still follow the underlying spin texture when it changes on the atomic scale. In Fig. 3(a), an SP-STM image of an DL Fe island prepared on an Ir(111) substrate is shown. Here, the electronic and magnetic information is encoded in the z channel, recorded via direct spin-polarized tunneling into the surface [21,30]. Two different kinds of strain-induced dislocation lines with different heights are observed on the Fe island [31]. In addition, a pattern with a period of 2 nm evolves along the dislocation lines, as shown in the inset of Fig. 3(a).

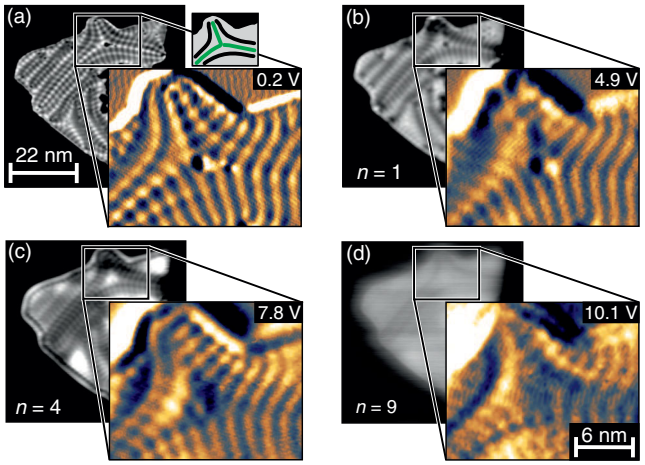

FIG. 3. Probing atomic-scale spin spirals with high-order RSs. Constant current map of a DL Fe/Ir(111) island, recorded (a) when tunneling directly into the surface ($U = 200$ mV), and (b)–(d) via tunneling into a RS (state order n and bias U as indicated). Dislocation lines with two different heights are schematically sketched in (a) (green and black lines). Insets: Closer view of the map (differentiated). A periodic pattern due to spin spirals propagating along the dislocation lines is observable. ($I = 1$ nA, $T = 30$ K.)

As has been shown by recent SP-STM studies, this pattern is the manifestation of a Néel-type spin spiral [31].

The same Fe island was imaged via spin-polarized tunneling into the first RS, as shown in Fig. 3(b). Whereas topographic features, like the atomic step edges and the dislocation lines, tend to smear out, the magnetic pattern remains visible, as shown in the inset of Fig. 3(b). Consequently, the first RS on the Fe island reflects the local spin quantization axis of the spin spiral. A bias-dependent series of SP-STM images of the same Fe island has been recorded via spin-polarized electron injection into higher-order RSs. Exemplary results for the fourth and nineth RS are shown in Fig. 3(c)–3(d). Here, the topographic features clearly fade away with increasing U, which is in agreement with previous observations in spin-averaged STM studies [32–34]. Interestingly, the magnetic pattern remains visible in all SP-STM images, thereby indicating that even higher-order RSs reflect the local spin quantization axis of the underlying spin texture that changes on the atomic scale.

A magnetic SP-STM image of an extended Fe DL film on Ir(111) is shown in Fig. 4(a). It was obtained via spin-polarized tunneling into the first RS above the Fe DL and recording the spatially resolved dI/dU signal. In contrast to the Fe DL island discussed before, here a regular magnetic pattern of spin spirals evolves on the film, with extended domains of propagation directions. Performing spectroscopy over a wide bias range up to $U = 20$ V reveals the energy positions of the first 31 RSs on the Fe film, as shown in Fig. 4(b). In Fig. 4(c), the local corrugations Δz on the spin spiral are shown, recorded by tunneling into the first and a high-order RS, respectively.

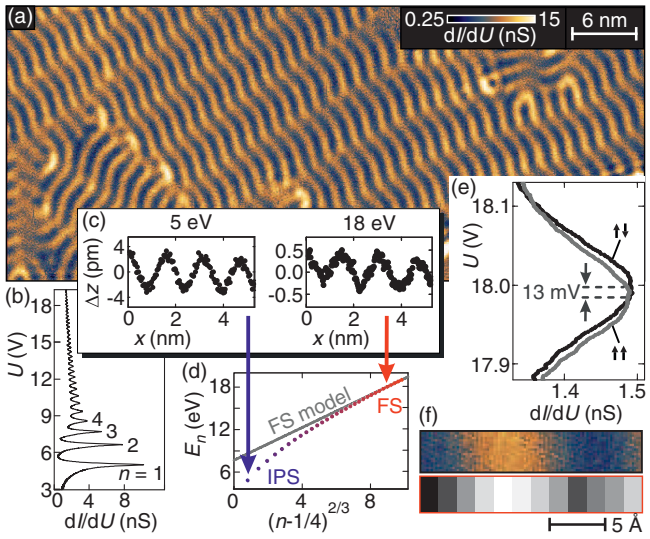

FIG. 4. Stark-shifted IPSs and FSs on atomic-scale spin spirals. (a) Magnetic dI/dU map of the DL Fe/Ir(111) spin spirals, imaged via the first RS ($U = 5.3$ V). (b) $dI/dU(U)$ revealing over 30 RSs on the DL Fe/Ir(111). (c) Spin-dependent corrugation Δz as a function of lateral position x, recorded via tunneling into the 1st (left) and 27th (right) RS (electron energy as indicated). (d) State energy E_n as a function of $(n-1/4)^{2/3}$, revealing the transition from Stark-shifted IPSs to FSs. (e) Spin-resolved dI/dU spectra of the FS at 18 eV, taken on surface sites with parallel and antiparallel alignment of tip and sample magnetization. (f) (Top) Magnetic map of the DL Fe/Ir(111) spin spiral ($U = 5$ V). (Bottom) Map of the spin-dependent phase shift ϕ_C for a spin-polarized electron with $E = 18$ eV upon reflection at the surface. ($I = 1$ nA, $T = 30$ K.)

Despite the considerable reduction of the corrugation with increasing U, the characteristic spin spiraling is clearly visible, even in the high-order RS at $eU = 18$ eV. The high-order RSs are expected to experience an almost triangular vacuum potential due to the electric field applied to the surface, therefore being called field states (FSs). Their positions in energy as a function of order n are proportional to $(n-1/4)^{2/3}$ [35]. In Fig. 4(d), the energies of the RSs up to order $n = 31$ are shown, as determined from the spectroscopy in Fig. 4(b). Obviously, the data reproduce the model of FS for high n, whereas a considerable deviation is observed for low-order RSs. For low n, the image potential has to be considered, resulting in shifting of the RSs to lower energies.

Consequently, our experimental study includes a variety of RSs, ranging from Stark-shifted IPSs at low energies to FSs at high energies. In common to all the investigated RSs is their atomic-scale sensitivity to the underlying noncollinear surface spin texture. Irrespective of the energy, the existence of a spin quantization axis that rotates with the surface spin is demonstrated, as exemplarily shown in Fig. 4(e) for a high-order FS. Here, two spectroscopy curves have been recorded around the FS at $U = 18$ V, once in the parallel and once in the antiparallel relative spin configuration between the tip and the sample. Likewise in Fig. 2(d), a shifting of the FS peak is observed, which is attributed to an effective splitting of approximately 13 meV. Spatially and spin-resolved spectroscopy reveals a significant exchange splitting for all investigated RSs between 4 and 14 meV [24].

The noncollinear magnetism in the systems investigated in our study is a consequence of the combined Heisenberg exchange, DM, and spin-orbit interactions [20,36]. For IPSs in the absence of an electric field, the influence of the Heisenberg exchange is well explored [15,16,27,28,37,38], while spin-orbit interactions on nonmagnetic Rashba systems have been revealed only recently [39–41]. Here, we demonstrate the impact of DM and spin-orbit interactions above the vacuum level on Stark-shifted IPS and FS in terms of magnetic noncollinearity in the RSs. Within the context of the phase accumulation model discussed above, we attribute the observed RS spin sensitivity to the atomic-scale nature of the spin-dependent electron reflection at the surface. The experimental findings imply that the resonance condition of Eq. (1) has to be fulfilled with a spin-dependent wave function phase shift ϕ_C that is set by the local spin quantization axis of the surface. Within a model for the FS regime, this spin-dependent ϕ_C can be calculated from the spectroscopic peak positions recorded along the spin spiral [24]. The resulting map of the spin-dependent ϕ_C upon reflection of an electron with $E = 18$ eV at the DL Fe/Ir(111) surface is shown in Fig. 4(f), together with a magnetic map of the respective surface area. Obviously, ϕ_C reveals a periodic modulation according to the underlying spin spiral. Consequently, our spin-resolved electron vacuum interferometer allows for mapping the spin-dependent electron wave function phase shift on the atomic scale. Since $\phi_C(E)$ is fully determined by the surface electronic band structure around E, its sensitivity to the noncollinear magnetism indicates that all the spin-dependent interactions that drive the magnetic ground state and are considered to be small (meV/atom) significantly affect the electronic surface band structure even far above E_{vac}. This implies that yet a free electron feels these interactions upon scattering at a magnetic surface or interface.

In conclusion, RSs are found to be atomic-scale probes for surface magnetism. Their local analysis by means of SP-STM provides an experimental approach for the detailed investigation of spin-dependent interactions between electrons above E_{vac} and surfaces with noncollinear spin textures.

Financial support from the Deutsche Forschungsgemeinschaft via Grants No. SCHL 2096/1-1 and No. SCHL 2096/1-2 is gratefully acknowledged.

*aschlenh@physnet.uni-hamburg.de
†Present address: Department of Materials, ETH Zurich, 8093 Zurich, Switzerland.

[1] P. Dey and W. Weber, J. Phys. Condens. Matter **23**, 473201 (2011).
[2] M. S. Altman, J. Phys. Condens. Matter **22**, 084017 (2010).
[3] F. J. dos Santos, M. dos Santos Dias, F. S. M. Guimarães, J. Bouaziz, and S. Lounis, Phys. Rev. B **97**, 024431 (2018).
[4] R. Zdyb and E. Bauer, Phys. Rev. B **96**, 205408 (2017).
[5] R. Zdyb and E. Bauer, Phys. Rev. Lett. **88**, 166403 (2002).
[6] M. S. Hammond, G. Fahsold, and J. Kirschner, Phys. Rev. B **45**, 6131 (1992).
[7] K. Bobrov, A. J. Mayne, and G. Dujardin, Nature (London) **413**, 616 (2001).
[8] A. J. Caamaño, Y. Pogorelov, O. Custance, J. Méndez, A. M. Baró, J. Y. Veuillen, J. M. Gómez-Rodríguez, and J. J. Sáenz, Surf. Sci. **426**, L420 (1999).
[9] N. V. Smith, Rep. Prog. Phys. **51**, 1227 (1988).
[10] P. M. Echenique and J. B. Pendry, J. Phys. C **11**, 2065 (1978).
[11] U. Höfer and P. Echenique, Surf. Sci. **643**, 203 (2016).
[12] G. Binnig, K. H. Frank, H. Fuchs, N. Garcia, B. Reihl, H. Rohrer, F. Salvan, and A. R. Williams, Phys. Rev. Lett. **55**, 991 (1985).
[13] S. Crampin, Phys. Rev. Lett. **95**, 046801 (2005).
[14] A. Hanuschkin, D. Wortmann, and S. Blügel, Phys. Rev. B **76**, 165417 (2007).
[15] M. Nekovee, S. Crampin, and J. E. Inglesfield, Phys. Rev. Lett. **70**, 3099 (1993).
[16] F. Passek, M. Donath, K. Ertl, and V. Dose, Phys. Rev. Lett. **75**, 2746 (1995).
[17] A. Schlenhoff, S. Krause, G. Herzog, and R. Wiesendanger, Appl. Phys. Lett. **97**, 083104 (2010).
[18] R. S. Becker, J. A. Golovchenko, and B. S. Swartzentruber, Phys. Rev. Lett. **55**, 987 (1985).
[19] A. Kubetzka, O. Pietzsch, M. Bode, and R. Wiesendanger, Phys. Rev. B **67**, 020401(R) (2003).
[20] S. Meckler, N. Mikuszeit, A. Preßler, E. Y. Vedmedenko, O. Pietzsch, and R. Wiesendanger, Phys. Rev. Lett. **103**, 157201 (2009).
[21] D. Wortmann, S. Heinze, P. Kurz, G. Bihlmayer, and S. Blügel, Phys. Rev. Lett. **86**, 4132 (2001).
[22] R. Wiesendanger, Rev. Mod. Phys. **81**, 1495 (2009).
[23] M. Bode, A. Kubetzka, S. Heinze, O. Pietzsch, R. Wiesendanger, M. Heide, X. Nie, G. Bihlmayer, and S. Blügel, J. Phys. Condens. Matter **15**, S679 (2003).
[24] See Supplemental Material at http://link.aps.org/supplemental/10.1103/PhysRevLett.123.087202 for the fitting of a domain wall model to the data for revealing the surface spin configuration, a detailed discussion of the spatially and spin-resolved spectroscopy, a discussion of the relation of intrinsic and effective exchange splitting of RSs, and the effective splitting of the RSs as a function of energy.
[25] A. Schlenhoff, S. Krause, A. Sonntag, and R. Wiesendanger, Phys. Rev. Lett. **109**, 097602 (2012).
[26] A. Kubetzka, M. Bode, and R. Wiesendanger, Appl. Phys. Lett. **91**, 012508 (2007).
[27] U. Thomann, C. Reuß, T. Fauster, F. Passek, and M. Donath, Phys. Rev. B **61**, 16163 (2000).
[28] M. Donath, C. Math, M. Pickel, A. B. Schmidt, and M. Weinelt, Surf. Sci. **601**, 5701 (2007).
[29] M. Julliere, Phys. Lett. **54A**, 225 (1975).
[30] R. Wiesendanger, H.-J. Güntherodt, G. Güntherodt, R. J. Gambino, and R. Ruf, Phys. Rev. Lett. **65**, 247 (1990).
[31] P.-J. Hsu, A. Finco, L. Schmidt, A. Kubetzka, K. von Bergmann, and R. Wiesendanger, Phys. Rev. Lett. **116**, 017201 (2016).
[32] P. Ruffieux, K. Aït-Mansour, A. Bendounan, R. Fasel, L. Patthey, P. Gröning, and O. Gröning, Phys. Rev. Lett. **102**, 086807 (2009).
[33] K. Schouteden and C. Van Haesendonck, Phys. Rev. Lett. **103**, 266805 (2009).
[34] H.-C. Ploigt, C. Brun, M. Pivetta, F. Patthey, and W.-D. Schneider, Phys. Rev. B **76**, 195404 (2007).
[35] T. Ando, A. B. Fowler, and F. Stern, Rev. Mod. Phys. **54**, 437 (1982).
[36] K. Bergmann, A. Kubetzka, O. Pietzsch, and R. Wiesendanger, J. Phys. Condens. Matter **26**, 394002 (2014).
[37] F. J. Himpsel, Phys. Rev. B **43**, 13394 (1991).
[38] M. Weinelt, A. B. Schmidt, M. Pickel, and M. Donath, Prog. Surf. Sci. **82**, 388 (2007).
[39] J. R. McLaughlan, E. M. Llewellyn-Samuel, and S. Crampin, J. Phys. Condens. Matter **16**, 6841 (2004).
[40] S. Tognolini, S. Achilli, L. Longetti, E. Fava, C. Mariani, M. I. Trioni, and S. Pagliara, Phys. Rev. Lett. **115**, 046801 (2015).
[41] R. Arafune, T. Nakazawa, N. Takagi, M. Kawai, and H. Ishida, Phys. Rev. Lett. **117**, 239701 (2016).